

NO₂ gas sensing of chromium doped nanostructured copper sulfide films prepared by spray pyrolysis method

H. S. Rasheed^a, K. M. Qader^b, K. N. Hussein^c, N. F. Habubi^d, S. S. Chiad^a,
N. M. Mirza^{a, *}, M. Jadan^{e, f}, Y. H. Kadhim^g

^aDepartment of Physics, College of Education, Mustansiriyah University, Iraq.

^bDepartment of Physics, College of Science, Mustansiriyah University, Iraq.

^cDepartment of Radiology, Al-Manara College for Medical Science, Iraq.

^dDepartment of Radiation and Sonar Technologies, Alnukhba University College, Iraq.

^eDepartment of Physics, College of Science, Imam Abdulrahman Bin Faisal University, P.O. Box 1982, 31441 Dammam, Saudi Arabia

^fBasic and Applied Scientific Research Center, Imam Abdulrahman Bin Faisal University, P.O. Box 1982, 31441 Dammam, Saudi Arabia

^gDepartment of Optics Techniques, College of Health and Medical Techniques, AL-Mustaqbal University, Babylon, Hillah, 51001, Iraq.

Undoped and Chromium (Cr) doped (2, 4%) copper sulfide (Cu₂S) nanostructured thin films were created by spray pyrolysis. The films were polycrystalline and combined cubic and monoclinic structures, according to the results of the XRD investigation. Surface roughness values for the doped and undoped thin films are 8.71, 7.79, and 3.24 nm, respectively. SEM images display Cu₂S nanostructures with fine crystallites and traces of nanorod. Chromium doping increases particle size and induces nanorod growth, enhancing surface porosity. The optical examination shows that Cr-doped Cu₂S thin films exhibit effective absorption ($> 10^4$ orders) in the visible range. From the change in absorption coefficient, it can be observed that there is a valley around 2.6 eV. By doping Cr (up to 2%) in Cu₂S films, it is possible to control the band gap between 2.62 eV and 2.73 eV. The refractive index of undoped Cu₂S films decreases with increasing Cr-doping concentration. Gas sensing of Chromium-doped and undoped Cu₂S nanostructures involves dynamic resistance change at 100°C. Undoped Cu₂S displays low resistance, exhibiting p-type semiconductor behavior. Notably, 4% Cr-doped Cu₂S shows high resistance, and the introduction of NO₂ decreases resistance. Decreased sensitivity with rising Cr doping in Cu₂S: 2% Cr and Cu₂S: 4% Cr. Responsiveness declined across different NO₂ concentrations (200 ppm, 300 ppm, and 400 ppm).

(Received March 15, 2024; Accepted June 4, 2024)

Keywords: Cu₂S, Cr, Thin films, Doping, Spray pyrolysis, Physical properties

1. Introduction

Copper sulfide is a significant metal-based sulfide thin film (Cu₂S). This is due to the substance's lesser toxicity than many other chalcogenides and the ease with which waste solutions may be managed for the environment. It may be used in various electrical applications [1]. One II-VI chalcogenide semiconductor with unique capabilities for photoelectric conversion is Cu₂S. The p-type semiconductor known as Cu₂S is an acceptor thanks to copper vacancies [2]. The direct and indirect band gaps of Cu₂S are 1.2 eV and 1.8 eV [3,4]. Various techniques were reported [5]. Due to their strong I.R. reflection and good transmission in the visible light spectrum, Cu₂S thin films are advantageous for solar cells. Due to its wide range of optical band gaps may be used in various applications, including photosensors, gas sensors, catalysts, and solar cells [6-8]. Cu₂S thin films are very attractive p-type materials from a technological standpoint. However, there is little knowledge of how doping affects the properties of Cu₂S thin films. This work produced thin films

* Corresponding author: nabeel.mirza@uomustansiriyah.edu.iq
<https://doi.org/10.15251/DJNB.2024.192.805>

of Cr-doped Cu₂S on glass slides using a simple spray pyrolysis method. Doping Cu₂S with the necessary components will change and adapt its physical characteristics. The doping enhances the host material's optical, electrical, and magnetic capabilities, which alters the intrinsic quantum energy levels to create discrete energy levels. To achieve high conductivity, it is crucial to comprehend the numerous interactions between acceptor and crystal defects, whether native or doped [9-11]. The impact of Cr doping on the optical characteristics of Cu₂S thin films has been studied. Cu₂S thin films are created using several different synthesis methods, such as spray pyrolysis [12–16], vacuum evaporation [17], chemical bath deposition (CBD) [18, 19], successive ionic layer adsorption and reaction (SILAR) [20, 21], chemical vapor deposition [22], atomic layer deposition (ALD) [23] and photochemical method [24]. This study explores doping's effects on the structural and optical characteristics of copper sulphide layer that was being deposited and the process of producing Cu₂S thin films using chemical spray pyrolysis (CSP).

2. Experimental

Thin films of undoped Cu₂S and Cu₂S: Cr were formed using an integrated spray pyrolysis coating equipment. (CuCl₂) (0.1M) dissolved in deionized water were combined to create the spray solution. Cr trichloride (CrCl₃) was dissolved in isopropyl alcohol and added to the solution to obtain Cr doping. The solution comprised 50 ml and had a doping concentration of (0, 2, 4) %. The requirements for preparation: 400°C was the substrate temperature, 29 cm was the distance between the spout and base, and 10⁵ Pas. of nitrogen gas was utilized as the carrier gas during the 9-second spraying time, which was extended by 85 seconds to prevent cooling. Using a weighing technique, the film's thickness was determined to be 340 ± 25 nm. The nature of film structure was ascertained using XRD, and the film surface that had been deposited was examined using AFM. The surface microstructure was examined using a Hitachi SEM (model S-4160). Using a UV-visible Shimadzu double-beam spectrophotometer, optical transmittance is obtained. Gas sensitivity is commonly evaluated based on the percentage change in film resistance after exposure. The specimens were positioned inside a custom-made cylindrical chamber (with a radius of 7.5 cm and a height of 15 cm) for testing.

3. Results and discussions

The XRD of Cu₂S produced on glass substrates at various Cr doping levels (0. 2 and 4) % is shown in Fig. 1. The glass substrate causes the noticeable hump in the 20°–70° range. The spectra essentially depict a Cu₂S sheet that is amorphous (no diffraction peaks are present in both spectra). The peaks of their crystalline structure, which correspond to the (111), (200) and (220) planes, respectively, at 2θ equal (27.51°, 31.82° and 45.49° are attributed to cubic structure. No secondary phases were seen after adding Cr ions to the Cu₂S system. However, the peak shift's strength gradually increases when the doping level rises. The outcomes demonstrated that Cr was incorporated into the Cu₂S system and that doping enhanced the compound's crystallinity. The ion radius of Cr³⁺ is 0.62, whereas that of Cu²⁺ is 0.73, which is coherent with the ionic radius of Cr concerning Cu. This is due to the different diameters of the two ion radii. Furthermore, due to the significant mismatch in our scenario, only a small amount of Cr⁺³ charge and Cu⁺² charge is present. Additionally, only a tiny amount of this (Cr) dopant could be tolerated by the Cu₂S structure. The diffusivity and growth rate are decreased because of the lower Cu content in the lattice due to higher Cr doping [12, 14].

Scherrer's formula, which is shown in Eq. 1 is used to compute the mean crystallite size, *D*. [25, 26]:

$$D = \frac{0.9 \lambda}{\beta \cos \theta} \quad (1)$$

where β is FWHM in radians and θ is Bragg's angle. To determine D of pure and Cr-doped Cu_2S thin films, the (200) plane was chosen. The XRD data's average crystallite size range of nanoparticles was between 14.1 and 16.31 nm. Table 1 demonstrates that the enhancement in crystal structure in the doped samples causes D of pure and Cr-doped Cu_2S thin films to rise when the concentration of Chromium is increased. Crystallite size allows for the calculation of dislocation density in the films. Dislocations are flaws in crystals that result from the lattice being misregistered in one area of the crystal relative to another. Dislocations are not equilibrium flaws, in contrast to vacancies and interstitial atoms [27, 28].

The following expression was used to evaluate the dislocation density (δ) [29, 30]:

$$\delta = \frac{1}{D^2} \text{ (line. m}^{-2}\text{)} \quad (2)$$

The microstrain (ϵ) was evaluated via the relation [31,32]:

$$\epsilon = \frac{\beta \cos \theta}{4} \quad (3)$$

Table 1 shows that the lattice parameter increases as the doping content increases, indicating the integration of Cr into the Cu_2S lattice. As the strain values drop, the doping concentration rises. The computed δ and ϵ are discovered to have an opposed trend. It is concluded that the lower and bigger D values demonstrate the films' improved crystallization. The crystallite first decreases at 0.02 M Cr-doping concentration and increases as the doping concentration rises. The loss of crystallinity with dopant causes a decrease in crystallite size [33, 34]. Increased strain and decreased peak intensity support this conclusion. More Cr atoms disperse Cu_2S and lessen the dislocations of the Cu_2S film, expanding the crystallite size as the Cr concentration is raised. Stress decreases with a rise in doping content when the Cr atoms settle in the film dislocations at higher concentrations [20].

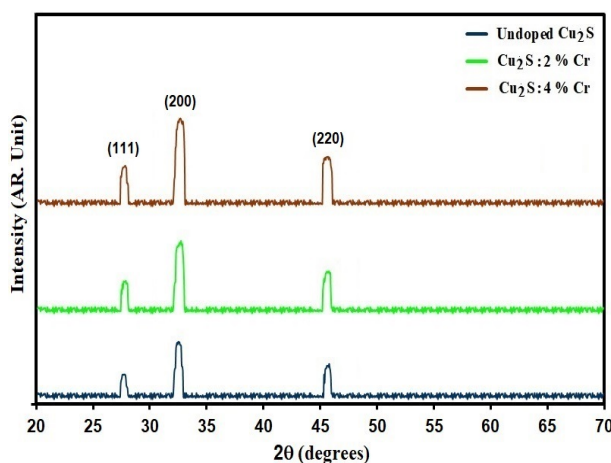


Fig. 1. XRD patterns of Undoped and Cr-doped Cu_2S films.

Table 1. Structure parameters of pure and Cr-doped Cu_2S films.

Specimen	2θ ($^\circ$)	(hkl) Plane	FWHM ($^\circ$)	Optical bandgap (eV)	Grain size (nm)	Dislocations density ($\times 10^{14}$) (lines/ m^2)	Strain ($\times 10^{-4}$)
Undoped Cu_2S	31.82	200	0.59	2.73	14.10	50.22	24.57
Cu_2S : 2% Cr	31.79	200	0.54	2.68	15.41	42.08	22.92
Cu_2S : 4% Cr	31.75	200	0.51	2.62	16.31	37.54	21.24

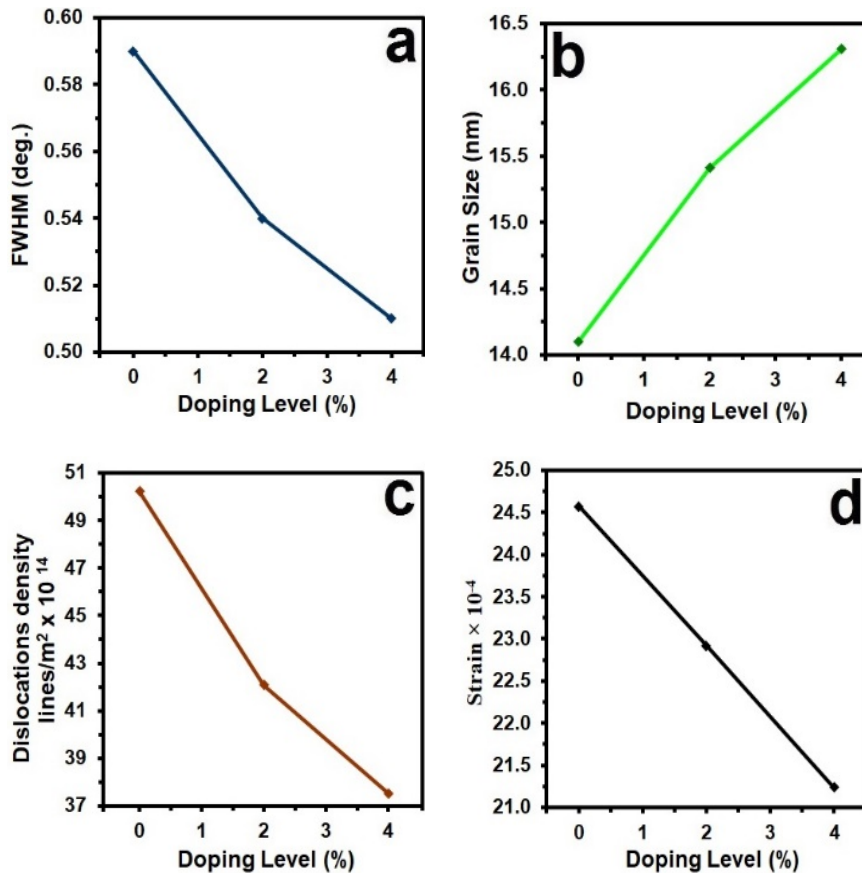


Fig. 2. X-ray parameters of pure and Cr-doped Cu_2S films.

Three-dimensional AFM scans of the crystalline Cu_2S thin films produced by CSP are shown in Figure 2. The surface is uneven and contains nanocrystals and shaped crystallites. With increased doping, Pav's average particle size falls from 88.78 nm to 51.3 nm, and the average roughness R_a falls from 6.91 nm to 3.67 nm. Compared to films created at the other undoped levels, the film prepared at 3% doping appears reasonably smooth. The root mean square (RMS) of the roughness of the Cu_2S thin films produced on glass substrates at various doping levels. The minimum RMS value in this example is 3.24 nm at 4% doping and 8.71 nm at undoped, indicating a higher surface quality level [17]. We can conclude that the Cu_2S : Cr preparation has a better value at 4% doping. This outcome is consistent with the characterizations from X-rays [35, 36].

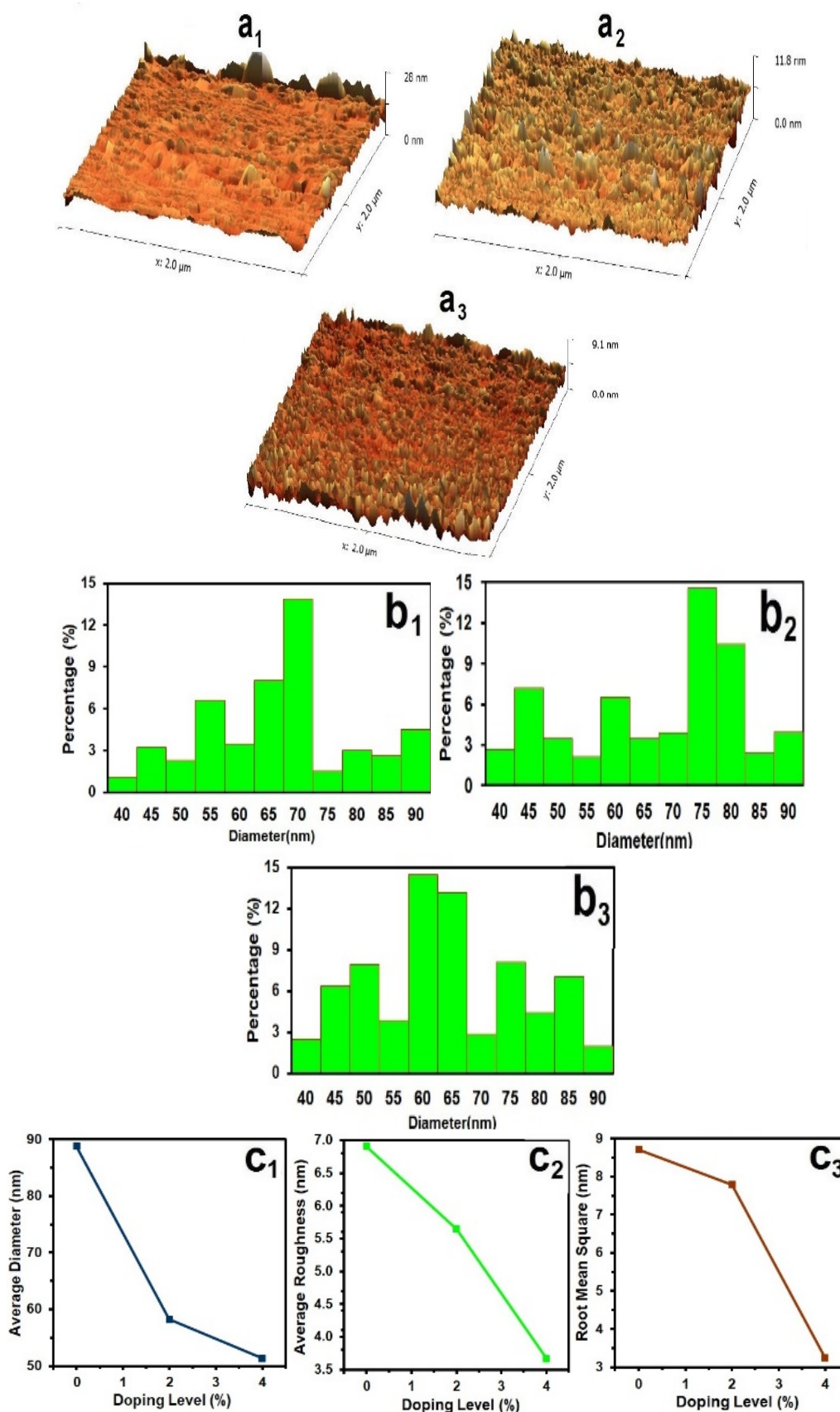


Fig. 3. AFM of pure and Cr-doped Cu₂S films.

Table 2. AFM parameter measurement of pure and Cr-doped Cu_2S films.

Samples	Average Particle size Nm	R_a (nm)	RMS (nm)
Undoped Cu_2S	88.78	6.91	8.71
Cu_2S : 2% Cr	58.2	5.64	7.79
Cu_2S : 4% Cr	51.3	3.67	3.24

The morphology of the Cu_2S nanostructures film, prepared through spray pyrolysis, is characterized using SEM images. Fig. (4) depicts the typical SEM images of the prepared Cu_2S nanostructures. The images reveal fine crystallites with traces of nanorods. No large particles are observed in the SEM images. The particle size increases from 103 nm to 154.15 nm as the Chromium doping rises from 0% Cr to 2% Cr, and nanorods grow perpendicularly with a diameter of 85 nm, rendering the surface more porous [15].

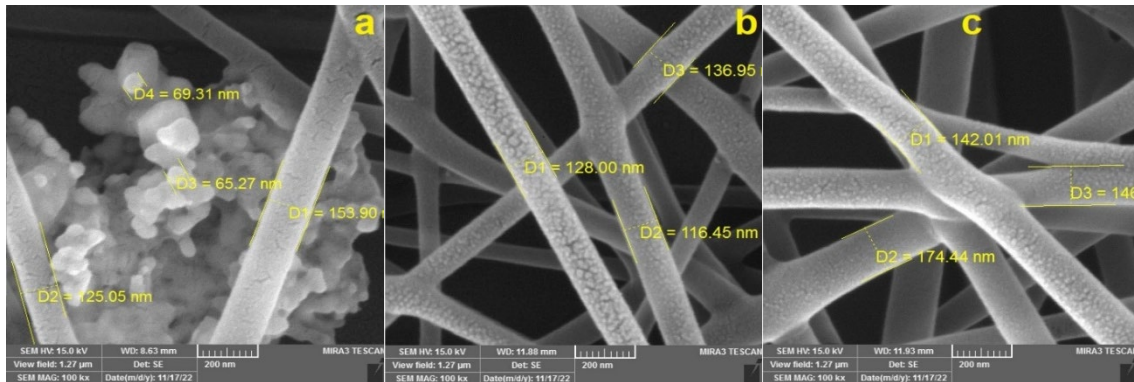


Fig. 4. SEM pattern for nanostructure Cu_2S prepared by spray pyrolysis (a) undoped Cu_2S ; (b) 2% doped by Cr. (c) 4% doped by Cr.

A visual examination of Cu_2S 2% and 4% thin films with undoped and cr-doped compositions was conducted at ambient temperature [37].

Experimental measurements are typically expressed in terms of the percentage transmittance (T), defined as [38]:

$$T\% = \frac{I}{I_0} \% \quad (4)$$

where (I) is the light intensity after it passes through the sample and (I_0) is the initial light intensity.

Figure 5 displays the transmittance (T) spectra of the intended films. The Figure shows that T is relatively low in the 500–750 nm wavelength area, climbs dramatically to its maximum between 550 and 750 nm, and then rapidly declines to become flat in the near-infrared region. These results agree with Mehdi et al. [12, 23]. Additionally, it has been shown that T declines with increasing Cr doping content, with 4% Cr-doped Cu_2S films having the lowest transmittance (about 60%) and undoped Cu_2S films having the highest transmittance (about 65%). The absorbance spectra of deposited Cu_2S thin films with various film doping are shown in Fig. 6. The same patterns are seen in all films, with more absorption on the shorter wavelength side. Due to the combination of Cu^{+2} and Cr^{+3} ions, which occurs due to the difference in ionic radii, this behavior may be linked to an increase in defects. These values produce suitable materials for solar cells. Due to the donor level in the thin film shifting toward the conduction band with increased

doping concentrations, the bandgap shifts towards lower energy. It can also result from developing defect states within the direct gap, which enhances the film's crystal structure. [36].

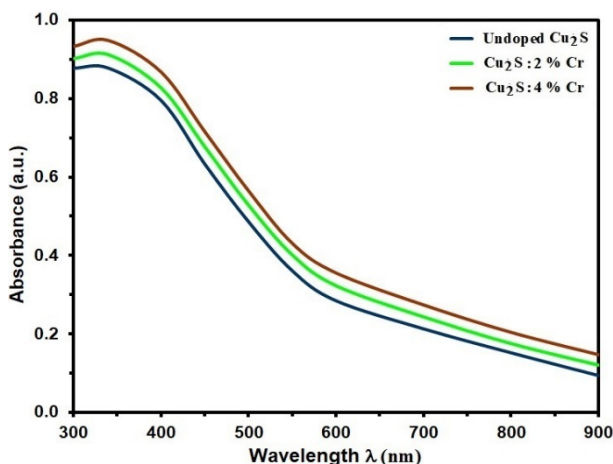


Fig. 5. *T* of grown film.

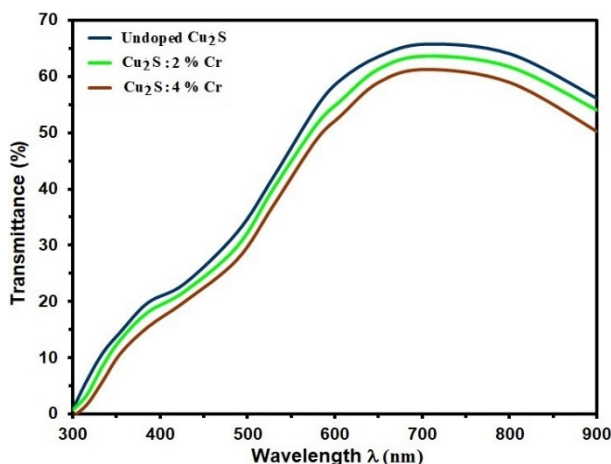


Fig. 6. Absorbance of the intended film.

The absorption coefficient (α) was calculated using the relation [37, 38]:

$$\alpha = 2.303 \frac{A}{t} \quad (5)$$

According to Figure 7, the absorption coefficient (α) has a high value (10^4) in the lower energy zone, drops to a minimum value at photon energies of around 2.62 eV, and then increases quickly as photon energies rise. The Figure also shows that it marginally rises with increasing Cr doping concentration; this finding may be related to the expansion of the optical band gap caused by Cr doping. Due to the donor level in the thin film shifting toward the conduction band with increased doping concentrations, the bandgap shifts towards lower energy [39, 40]. Another reason might be the development of defect states within the direct gap, which enhances the film's crystal structure [41]. This finding suggests that Cu₂S films effectively absorb light in the visible range and that their absorbance somewhat rises with Cr doping. Cu₂S films had a similar outcome, as found by [42, 43].

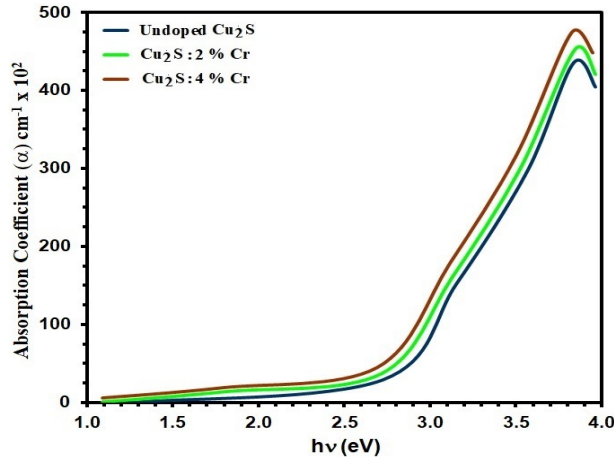


Fig. 7. α of the intended films.

The relationship below calculates the optical band gap, E_g . [44, 45].

$$(\alpha h\nu) = A(h\nu - E_g)^{1/2} \tag{6}$$

where A is the constant, $h\nu$ is the incident photon energy, and n is an exponent determining the optical absorption process. The absorption coefficient in this instance is in the range of 10^{-4} cm^{-1} , supporting the direct bandgap nature of the material. Tauc's plot is created using the optical absorption data, and there is a straightforward transition since the plot is linear. The relationship shown below is used to calculate the optical band gap E_g . As deposition doping increased, the energy gap of the thin films that were deposited shrunk. According to Figure 8, the crystallite size increase causes the energy gap to close as doping levels rise. As a result, the bandgap narrows, and the optical absorption edge moves toward longer wavelengths, increasing the absorption [46]. Compared to published data, this E_g value is one of the greatest bandgap values for Cu_2S . The tiny crystallite sizes associated with the "quantum size effect" are to blame for the greater bandgap value [47].

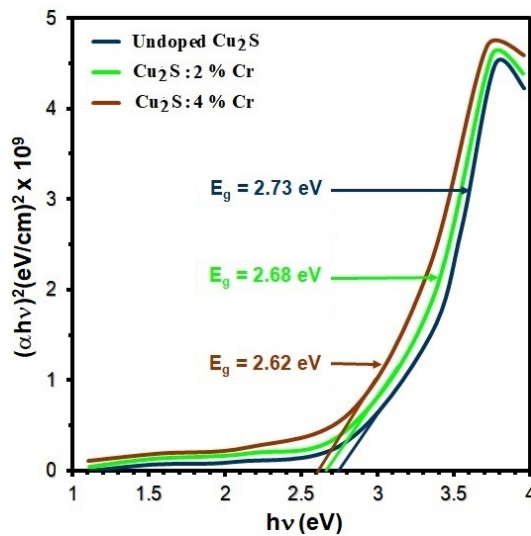


Fig. 8. E_g of the grown films.

The extinction coefficient (k) was calculated at different wavelengths using the relation (6) [48, 49]:

$$K = \frac{\alpha\lambda}{4\pi} \quad (7)$$

The refractive index (n) was calculated at different wavelengths using the relation (7) [50, 51]:

$$n = \frac{1+R^{\frac{1}{2}}}{1-R^{\frac{1}{2}}} \quad (8)$$

The n behaviour for the films (Cu_2S , $\text{Cu}_2\text{S}:2\%\text{Cr}$, and $\text{Cu}_2\text{S}:4\%\text{Cr}$) is depicted in Figure (9). This graph demonstrates how refractive index values fluctuate across the structural properties of films, falling after doping and rising at (300-550) nm. Figure (10), which depicts the variation of K with wavelength of the intended films shows that the extinction coefficient values decrease after doping. K values are similar to that of α for all ranges of the wavelength spectrum. This action can be attributed to an increase in defects due to the combination of Cu^{+2} ions and Cr^{+3} ions due to the difference in ionic radii [22].

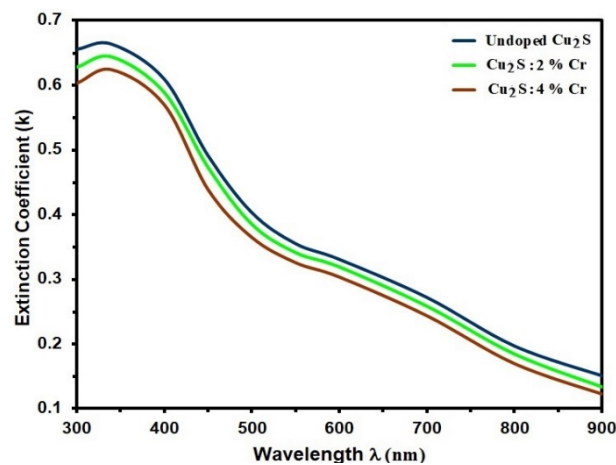


Fig. 9. n of the grown films.

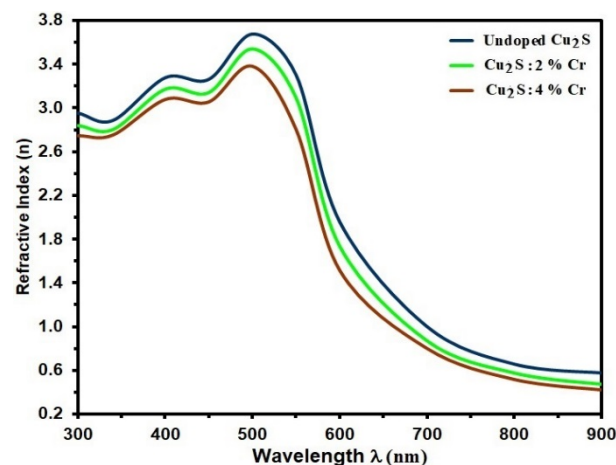


Fig. 10. K of the intended films.

The gas sensing properties of both Chromium-doped and undoped Cu₂S nanostructures were investigated for NO₂ as an oxidizing gas and a reduced gas. The dynamic resistance changes of the Cu₂S films, including undoped and Chromium-doped samples, was examined at an operating temperature of 100°C. Figure (11) illustrates the dynamic resistance change of the Cu₂S films when exposed to oxidizing gas (NO₂) at a concentration of 400 ppm. Notably, the undoped Cu₂S samples exhibited the lowest resistance. This can be attributed to the highest roughness observed in the AFM analysis and the increased surface area and porosity evident in the SEM images. The electrical resistance data further supports the observation that undoped Cu₂S films show the lowest resistance [52]. All samples exhibited p-type semiconductor behavior. Notably, the Cu₂S film with 4% Cr doping demonstrated the highest resistance. This can be attributed to the extraction of electrons from ionized donors through the conduction band, increasing the density of majority charge carriers (holes) at gas–solid interface. Consequently, the potential barrier for electrons decreases with the rising density of oxygen ions on the surface. The depletion layer and potential barrier contribute to a decrease in electrical resistivity, a parameter strongly influenced by the concentration of adsorbed oxygen ions on the surface [19]. The introduction of NO₂ ambient alters the concentration of these ions, leading to a decrease in resistance.

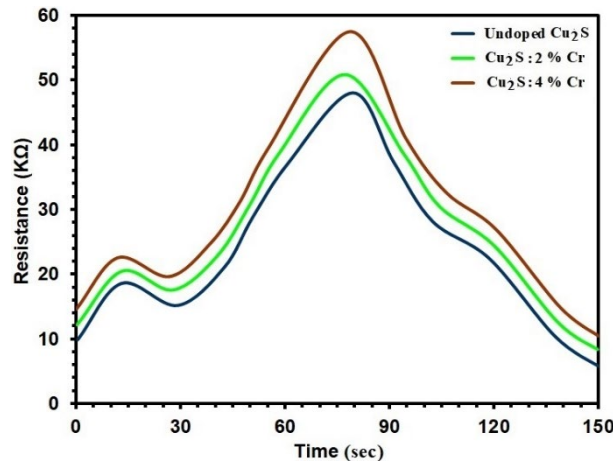


Fig. 11. Resistance as a function of operating time for Cu₂S and Cr-doped Cu₂S Films.

The sensitivity can be computed using equation (5) [52]:

$$Sensitivity = \frac{\Delta R}{R_g} = \left| \frac{R_g - R_a}{R_g} \right| \times 100 \% \quad (9)$$

where R_g = resistance of the film sensor in the presence of air
 R_a = resistance of the film sensor in the presence of gas.

The sensitivity plots in Figure (12) illustrate the impact of Undoped, Cu₂S: 2% Cr and Cu₂S: 4% Cr, on NO₂ gas exposure. The recombination process between charge carriers influences sensitivity, revealing a reduction with increasing Cr doping [36]. For varied Undoped, Cu₂S: 2% Cr and Cu₂S: 4% Cr, sensitivity decreased from 48.7 % to 11.6 % (200 ppm), 53.6 % to 14.0 % (300 ppm), and 58.8 % to 15.9 % (400 ppm) [50]. Sensitivity decreased for Undoped, Cu₂S: 2% Cr, and Cu₂S: 4% Cr, indicating that higher Cr doping levels led to a decline in the sensor's responsiveness to NO₂ gas [20].

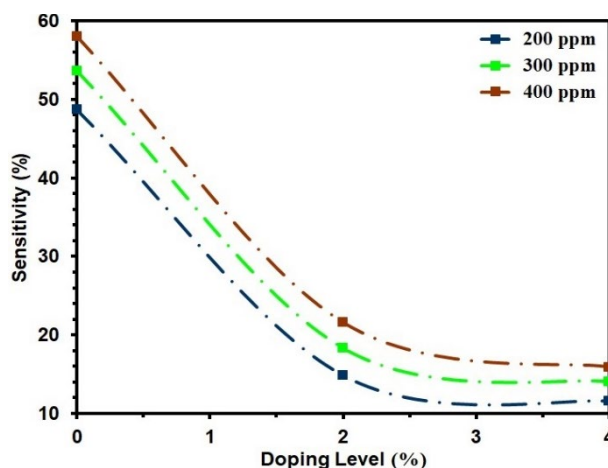


Fig. 12. Sensitivity of undoped and $\text{Cu}_2\text{S}:\text{Cr}$ films with different dopants.

4. Conclusion

The chemical spray pyrolysis approach effectively deposited undoped Cu_2S and Cr-doped Cu_2S thin films on glass substrates. XRD verified the cubic and hexagonal structures of the deposited films. Cu_2S film with Cr-doping displayed a densely packed, flower-like morphology on the AFM. Roughness and formed crystallites are seen on the surface. With increased doping, the average particle size falls from 88.78 nm to 51.3 nm, and the average roughness falls from 6.91 nm to 3.67 nm. SEM images show fine crystallites with traces of nanorods. Chromium doping increases particle size and induces nanorod growth, enhancing surface porosity. Further doping results in larger nanorods. The UV-Vis absorption spectra's low absorption between 300 and 550 nm revealed the film's high transparency in the visible spectrum.

The larger crystallite size, which results from less photon scattering by the crystallite borders, accounts for the observed improved optical transmittance of Cr-doped Cu_2S film. The increased charge carriers caused by adding Cr-doping caused the energy gap in Cu_2S to move from 2.62 eV (undoped) to 2.73 eV (Cr-doped). For gas sensing of Chromium-doped and undoped Cu_2S nanostructures, dynamic resistance changes at 100°C; undoped Cu_2S shows low resistance. P-type semiconductor behavior noted. 4% Cr-doped Cu_2S exhibits high resistance. NO_2 show a decrease in resistance. Reduced sensitivity with increased Cr doping in Undoped, $\text{Cu}_2\text{S}:\text{2\% Cr}$, and $\text{Cu}_2\text{S}:\text{4\% Cr}$. Decreased responsiveness was observed at various NO_2 concentrations (200 ppm, 300 ppm, and 400 ppm).

Acknowledgements

Mustansiriyah University and Al-Nukhba University College are responsible for this work.

References

- [1] M. Orphanou, E. Leontidis, T. Kyprianidou-Leodidou, P. Koutsoukos, K.C. Kyriacou, *Langmuir*. 20, 5605–5612 (2004); <https://doi.org/10.1021/la036372d>
- [2] X.-H. Liao, N.-Y. Chen, S. Xu, S.-B. Yang, J.-J. Zhu, *J. Cryst. Growth*. 252, 593–598 (2003); [https://doi.org/10.1016/s0022-0248\(03\)01030-3](https://doi.org/10.1016/s0022-0248(03)01030-3)
- [3] G. Liu, T. Schulmeyer, J. Brotz, A. Klein, W. Jaegermann, *Thin Solid Films*. 431, 477–482 (2003); [https://doi.org/10.1016/s0040-6090\(03\)00190-1](https://doi.org/10.1016/s0040-6090(03)00190-1)

- [4] A. Cuevas, R. Romero, D. Leinen, E.A. Dalchiele, J.R. Ramos-Barrado, F. Martin, *Sol Energ Mat Sol C*. 134, 199–208(2015); <https://doi.org/10.1016/j.solmat.2014.11.048>
- [5] F. H. Jasim, H. R. Shakir, S. S. Chiad, N. F. Habubi, Y. H. Kadhi, Jadan, M., *Digest Journal of Nanomaterials and Biostructures*, 18(4), 1385–1393 (2023); <https://doi.org/10.15251/DJNB.2023.184.1385>
- [6] S. Bagul, S. Chavhan, R. Sharma, *J. Phys. Chem. Solids*. 68,1623–1629 (2007); <https://doi.org/10.1016/j.jpcs.2007.03.053>
- [7] M. Xin, K. Li, H. Wang, *Appl. Surf. Sci.* 256, 1436–1442(2009); <https://doi.org/10.1016/j.apsusc.2009.08.104>
- [8] F. Zhuge, X. Li, X. Gao, X. Gan, F. Zhou, *Mater. Lett.* 63,652–654 (2009); <https://doi.org/10.1016/j.matlet.2008.12.010>
- [9] H. Pathan, C. Lokhande, *Bull. Mater. Sci.* 27, 85–111 (2004); <https://doi.org/10.1007/bf02708491>
- [10] F. A. Jasima, Z. S. A. Mosa, N. F. Habubi, Y. H. Kadhim, S. S. Chiad, *Digest Journal of Nanomaterials and Biostructures*, 18 (3), 1039–1049 (2023); <https://doi.org/10.15251/DJNB.2023.183.1039>
- [11] A. A. Abdul Razaq, F. H. Jasim, S. S. Chiad, F. A. Jasim, Z. S. A. Mosa, Y. H. Kadhim, *Journal of Ovonic Research*, 20 (2), 131 – 141 (2024); <https://doi.org/10.15251/JOR.2024.202.131>
- [12] H. Derin, *Appl Phys A*. 3, 839–845 (2014); <https://doi.org/10.1007/s00339-013-7695-2>
- [13] J. Madarasz, M. Okuya, S. Kaneko, *J. Eur. Ceram. Soc.* 21,2113–2116 (2001); [https://doi.org/10.1016/S0955-2219\(01\)00183-2](https://doi.org/10.1016/S0955-2219(01)00183-2)
- [14] S.-Y. Wang, W. Wang, Z.-H. Lu, *Mater. Sci. Eng. B*. 103, 184–188 (2003); [https://doi.org/10.1016/S0921-5107\(03\)00199-5](https://doi.org/10.1016/S0921-5107(03)00199-5)
- [15] L. Isac, A. Duta, A. Kriza, I. Enesca, M. Nanu, *J. Phys. Conf.Ser.* 61, 477–481 (2007); <https://doi.org/10.1088/1742-6596/61/1/096>
- [16] M. Adelifard, H. Eshghi, M.M.B. Mohagheghi, *Appl. Surf. Sci.*258, 5733–5738 (2012); <https://doi.org/10.1016/j.apsusc.2012.02.079>
- [17] L. Isac, L. Andronic, A. Enesca, A. Duta, *J. Photochem.Photobiol. A Chem.* 252, 53–59 (2013); <https://doi.org/10.1016/j.jphotochem.2012.11.011>
- [18] N. K. Allouche, T.B. Nasr, C. Guasch, N.K. Turki, *C. R. Chim.*13, 1364–1369 (2010); <https://doi.org/10.1016/j.crci.2010.04.012>
- [19] A. Ubale, D. Choudhari, J. Kantale, V. Mitkari, M. Nikam, W.Gawande, P. Patil, *J. Alloys Compd.* 509, 9249–9254 (2011); <https://doi.org/10.1016/j.jallcom.2011.07.009>
- [20] A.L. Abdelhady, K. Ramasamy, M.A. Malik, P. O'Brien, S.J.Haigh, J. Raftery, *J. Mater. Chem.* 21, 17888–17895 (2011); <https://doi.org/10.1039/C1JM13277F>
- [21] S. Sartale, C. Lokhande, *Mater. Chem. Phys.* 65, 63–67 (2000); [https://doi.org/10.1016/S0254-0584\(00\)00207-8](https://doi.org/10.1016/S0254-0584(00)00207-8)
- [22] H. Pathan, J. Desai, C. Lokhande, *Appl. Surf. Sci.* 202, 47–56(2002); [https://doi.org/10.1016/S0169-4332\(02\)00843-7](https://doi.org/10.1016/S0169-4332(02)00843-7)
- [23] J. Johansson, J. Kostamo, M. Karppinen, L. Niinisto, *J. Mater.Chem.* 12, 1022–1026 (2002); <https://doi.org/10.1039/B105901G>
- [24] A.A. Sagade, R. Sharma, *Sens. Actuators A Chem.* 133, 135–143(2008); <https://doi.org/10.1016/j.snb.2008.02.015>
- [25] N. Y. Ahmed, B. A. Bader, M. Y. Slewa, N. F. Habubi, S. S. Chiad, *NeuroQuantology*, 18(6), 55-60 (2020); <https://doi.org/10.1016/j.jlumin.2021.118221>
- [26] A. J. Ghazai, O. M. Abdulmunem, K. Y. Qader, S. S. Chiad, N. F. Habubi, *AIP Conference Proceedings* 2213 (1), 02010 1(2020); <https://doi.org/10.1063/5.0000158>
- [27] H. A. Hussin, R. S. Al-Hasnawy, R. I. Jasim, N. F. Habubi, S. S. Chiad, *Journal of Green Engineering*, 10(9), 7018-7028 (2020); <https://doi.org/10.1088/1742-6596/1999/1/012063>
- [28] S. S. Chiad, H. A. Noor, O. M. Abdulmunem, N. F. Habubi, M. Jadan, J. S. Addasi, *Journal of Ovonic Research*, 16 (1), 35-40 (2020). <https://doi.org/10.15251/JOR.2020.161.35>

- [29] H. T. Salloom, E. H. Hadi, N. F. Habubi, S. S. Chiad, M. Jadan, J. S. Addasi, *Digest Journal of Nanomaterials and Biostructures*, 15 (4), 189-1195 (2020); <https://doi.org/10.15251/DJNB.2020.154.1189>
- [30] R. S. Ali, N. A. H. Al Aaraji, E. H. Hadi, N. F. Habubi, S. S. Chiad, *Journal of Nanostructures* this link is disabled, 10(4), 810–816 (2020); <https://doi: 10.22052/jns.2020.04.014>
- [31] A. A. Khadayeir, R. I. Jasim, S. H. Jumaah, N. F. Habubi, S. S. Chiad, *Journal of Physics: Conference Series*, 1664 (1) (2020); <https://doi.org/10.1088/1742-6596/1664/1/012009>
- [32] S. S. Chiad, A. S. Alkelaby, K. S. Sharba, *Journal of Global Pharma Technology*, 11 (7), 662-665, (2020); <https://doi.org/10.1021/acscatal.1c01666>
- [33] Chiad, S.S., Noor, H.A., Abdulmunem, O.M., Habubi, N.F., *Journal of Physics: Conference Series* 1362(1), 012115 (2019); <https://doi.org/10.1088/1742-6596/1362/1/012115>
- [34] R. S. Ali, M. K. Mohammed, A. A. Khadayeir, Z. M. Abood, N. F. Habubi and S. S. Chiad, *Journal of Physics: Conference Series*, 1664 (1), 012016 (2020); <https://doi:10.1088/1742-6596/1664/1/012016>
- [35] A. S. Al Rawas, M. Y. Slewa, B. A. Bader, N. F. Habubi, S. S. Chiad, *Journal of Green Engineering*, 10 (9), 7141-7153 (2020); <https://doi.org/10.1021/acsami.1c00304>
- [36] R. S. Ali, H. S. Rasheed, N. F. Habubi, S.S. Chiad, *Chalcogenide Letters*, 20 (1), 63–72 (2023); <https://doi.org/10.15251/CL.2023.201.63>
- [37] K. Y. Qader, R. A. Ghazi, A. M. Jabbar, K. H. Abass, S. S. Chiad, *Journal of Green Engineering*, 10 (10), 7387-7398 (2020); <https://doi.org/10.1016/j.jece.2020.104011>
- [38] A. Ghazai, K. Qader, N. F. Hbubi, S. S. Chiad, O. Abdulmunem, *IOP Conference Series: Materials Science and Engineering*, 870 (1), 012027 (2020); <https://doi.org/ 10.1088/1757-899X/870/1/012027>
- [39] B. A. Bader, S. K. Muhammad, A. M. Jabbar, K. H. Abass, S. S. Chiad, N. F. Habubi, *J. Nanostruct*, 10 (4): 744-750, (2020); <https://doi.org/ 10.22052/JNS.2020.04.007>
- [40] O. M. Abdulmunem, A. M. Jabbar, S. K. Muhammad, M. O. Dawood, S. S. Chiad, N. F. Habubi, *Journal of Physics: Conference Series*, 1660 (1), 012055 (2020); <https://doi.org/ 10.1088/1742-6596/1660/1/012055>
- [41] E. H. Hadi, M. A. Abbsa, A. A. Khadayeir, Z. M. Abood, N. F. Habubi, and S.S. Chiad, *Journal of Physics: Conference Series*, 1664 (1), 012069 (2020); <https://doi.org/ 10.1088/1742-6596/1664/1/012069>
- [42] R. I. Jasim, E. H. Hadi, S. S. Chiad, N. F. Habubi, M. Jadan, J. S. Addasi, *Journal of Ovonic Research*, 19 (2), 187 – 196 (2023)..
- [43] N. N. Jandow, M. S. Othman, N. F. Habubi, S. S. Chiad, K. A. Mishjil, I. A. Al-Baidhany, *Materials Research Express*, 6 (11), (2020); <https://doi.org/10.1088/2053-1591/ab4af8>
- [44] M. S. Othman, K. A. Mishjil, H. G. Rashid, S. S. Chiad, N. F. Habubi, I. A. Al-Baidhany, *Journal of Materials Science: Materials in Electronics*, 31(11), 9037-9043 (2020); <https://doi.org/10.1007/s10854-020-03437-0>
- [45] E. S. Hassan, K. Y. Qader, E. H. Hadi, S. S. Chiad, N. F. Habubi, K. H. Abass, *Nano Biomedicine and Engineering*, 12(3), pp. 205-213 (2020); <https://doi.org/10.5101/nbe.v12i3.p205-213>
- [46] E. H. Hadi, D. A. Sabur, S. S. Chiad, N. F. Habubi, K., Abass, *Journal of Green Engineering*, 10 (10), 8390-8400 (2020); <https://doi.org/10.1063/5.0095169>
- [47] K. S. Sharba, A. S. Alkelaby, M. D. Sakhil, K. H. Abass, N. F. Habubi, S. S. Chiad, Enhancement of urbach energy and dispersion parameters of polyvinyl alcohol with Kaolin additive, *NeuroQuantology*, 18 (3), 66-73 (2020); <https://doi.org/10.14704/NQ.2020.18.3.NQ20152>
- [48] M. D. Sakhil, Z. M. Shaban, K. S. Sharba, N. F. Habub, K. H. Abass, S. S. Chiad, A. S. Alkelaby, *NeuroQuantology*, 18 (5), 56-61 (2020); <https://doi.org/10.14704/nq.2020.18.5.NQ20168>
- [49] Khadayeir, A. A., Hassan, E. S., Mubarak, T. H., Chiad, S.S., Habubi, N. F., Dawood, M.O., Al-Baidhany, I. A., *Journal of Physics: Conference Series*, 1294 (2) 022009(2019); <https://doi.1088/1742-6596/1294/2/022009>

- [50] H.T. Salloom, R. I. Jasim, N. F. Habubi, S. S. Chiad, M. Jadan, J. S. Addasi, Chinese Physics, 30 (6), 068505 (2021); <https://doi.org/10.1088/1674-1056/abd2a7>
- [51] K. Y. Qader, E. H. Hadi, N. F. Habubi, S. S. Chiad, M. Jadan, J. S. Addasi, International Journal of Thin Films Science and Technology, 10 (1), 41-44 (2021); <https://doi.org/10.18576/ijtfst/100107>
- [52] S. Zhao, G. Han, M. Li, Materials Chemistry and Physics, 120, 431-437 (2010); <https://doi.org/10.1016/j.matchemphys.2009.11.025>